

Microwave sol-gel synthesis of microcrystalline $\text{CaGd}_2(\text{MoO}_4)_4:\text{Er}^{3+}/\text{Yb}^{3+}$ phosphors and their upconversion photoluminescence properties

Chang Sung Lim¹, Victor Atuchin^{2,3,4,*}, Aleksandr Aleksandrovsky^{5,6}, Maxim Molokeev^{7,8},
Aleksandr Oreshonkov^{6,9}

¹Department of Advanced Materials Science & Engineering, Hanseo University, Seosan 356-706, Republic of Korea

²Laboratory of Optical Materials and Structures, Institute of Semiconductor Physics, SB RAS, Novosibirsk 630090, Russia

³Functional Electronics Laboratory, Tomsk State University, Tomsk 634050, Russia

⁴Laboratory of Semiconductor and Dielectric Materials, Novosibirsk State University, Novosibirsk 630090, Russia

⁵Laboratory of Coherent Optics, Kirensky Institute of Physics, SB RAS, Krasnoyarsk 660036, Russia

⁶Department of Photonics and Laser Technologies, Siberian Federal University, Krasnoyarsk 660079, Russia

⁷Laboratory of Crystal Physics, Kirensky Institute of Physics, SB RAS, Krasnoyarsk 660036, Russia

⁸Department of Physics, Far Eastern State Transport University, Khabarovsk 680021, Russia

⁹Laboratory of Molecular Spectroscopy, Kirensky Institute of Physics, SB RAS, Krasnoyarsk 660036, Russia

*Corresponding author: E-mail address: atuchin@isp.nsc.ru

Abstract

$\text{CaGd}_2(\text{MoO}_4)_4:\text{Er}^{3+}/\text{Yb}^{3+}$ phosphors with the doping concentrations of Er^{3+} and Yb^{3+} ($x = \text{Er}^{3+} + \text{Yb}^{3+}$, $\text{Er}^{3+} = 0.05, 0.1, 0.2$ and $\text{Yb}^{3+} = 0.2, 0.45$) have been successfully synthesized by the microwave sol-gel method, and the crystal structure refinement and upconversion photoluminescence properties have been investigated. The synthesized particles, being formed after heat-treatment at 900°C for 16 h, showed a well crystallized morphology. Under the excitation at 980 nm, $\text{CaGd}_2(\text{MoO}_4)_4:\text{Er}^{3+}/\text{Yb}^{3+}$ particles exhibited strong 525-nm and 550-nm emission bands in the green region and a weak 655-nm emission band in the red region. The Raman spectrum of undoped $\text{CaGd}_2(\text{MoO}_4)_4$ revealed about 15 narrow lines. The strongest band observed at 903 cm^{-1} was assigned to the ν_1 symmetric stretching vibration of MoO_4 tetrahedrons. The spectra of the samples doped with Er and Yb obtained under 514.5 nm excitation were dominated by Er^{3+} luminescence preventing the recording Raman spectra of these samples. Concentration quenching of the erbium luminescence at ${}^2\text{H}_{11/2} \rightarrow {}^4\text{I}_{15/2}$ and ${}^4\text{S}_{3/2} \rightarrow {}^4\text{I}_{15/2}$ transitions in the $\text{CaGd}_2(\text{MoO}_4)_4:\text{Er}^{3+}/\text{Yb}^{3+}$ crystal structure was established to be approximately at the 10 at.% doping level.

Key words: molybdate; sol-gel synthesis; upconversion; XRD; Raman

*Corresponding author. E-mail: atuchin@isp.nsc.ru

1. Introduction

Oxide photoluminescence materials are of great importance in modern photonic technology because of a great diversity of available phosphors with different compositions and spectroscopic properties, high operation durability and emission efficiency, and a pronounced chemical stability in the air environment [1-9]. Recently, rare-earth-doped upconversion (UC) photoluminescence particles have attracted great attention as functional materials for the frequency conversion from near infrared radiation of low photon energy to visible high photon energy radiation [10-17]. The UC photoluminescence particles have shown potential applications in various fields including biomedical imaging owing to their unique UC optical behavior that offer an improved light penetration depth, high chemical and photo stability, as well as the absence of auto-fluorescence during imaging, sharp emission bands and high resistance to photobleaching, which overcome the current limitations in traditional photoluminescence materials [12,15,17-20].

The double molybdate compounds with a general composition of $MB_2(MoO_4)_4$ (M: alkaline-earth or bivalent rare-earth metal ion, B: trivalent rare-earth or actinide ion) belong to a group of double alkaline earth lanthanide molybdates. With the decrease of the alkaline-earth metal ion radii ($R_{Ca} < R_{Sr} < R_{Ba}$; R = ionic radius), the structure of $MB_2(MoO_4)_4$ could be transformed from the monoclinic structure to a highly disordered tetragonal scheelite-type structure. As it can be reasonably supposed, the trivalent rare-earth ions in the disordered tetragonal-phase could be partially substituted by Er^{3+} and Yb^{3+} ions, and the ions are efficiently doped into the tetragonal phase crystal lattice due to similar radii of trivalent rare-earth ions B^{3+} , that results in the excellent UC photoluminescence properties [21-23]. Among rare-earth ions, the Er^{3+} ion is suitable for the infrared to visible light conversion through the UC process due to a proper electronic energy level configuration. The co-doped Yb^{3+} ions can remarkably enhance the UC yield due to the efficient energy transfer from Yb^{3+} to Er^{3+} . The Yb^{3+} ion, as a sensitizer, can be excited by incident infrared light source, then the energy is transferred to the Er^{3+} ion activator from which the visible radiation

can be emitted. The Er^{3+} ion activator is the luminescence center of the UC particles, while the sensitizer enhances the UC luminescence efficiency [24-26].

The rare-earth activated double molybdates have attracted great attention because of their spectroscopic characteristics and excellent UC photoluminescence properties. Several processes have been developed to prepare the rare-earth-doped double molybdates, including solid-state reactions [27-32], co-precipitation [33, 34], the sol-gel method [21-23], hydrothermal method [35, 36], Pechini method [37, 38], organic gel-thermal decomposition [39] and the microwave-assisted hydrothermal method [40]. For practical application of UC photoluminescence in products such as lasers, three-dimensional displays, light-emitting devices, and biological detectors, the features, such as homogeneous UC particle size distribution and morphology, need to be well defined. Usually, double molybdates are prepared by a solid-state method that requires high temperatures, lengthy heating process and subsequent grinding, which may occasionally result in a loss of the emission intensity. The sol-gel process possesses some advantages including good particle homogeneity, low calcination temperature and a small particle size, and a narrow particle size distribution promising for good luminescent characteristics. However, the sol-gel process has a disadvantage of long gelation time. As compared to the usual methods, microwave synthesis has its advantages of a very short reaction time, small-size particles, narrow particle size distribution and a high purity of the final polycrystalline products. Microwave heating is delivered to the material surface by radiant and/or convection heating which is transferred to the bulk of the material via conduction [41, 42]. Thus, the microwave sol-gel process is a cost-effective method that provides its high homogeneity with an easy scale-up, and it is emerging as a viable alternative approach for the synthesis of high-quality luminescent materials in short time periods. However, earlier, the synthesis of $\text{CaGd}_2(\text{MoO}_4)_4:\text{Er}^{3+}/\text{Yb}^{3+}$ phosphors by the microwave sol-gel process has not been reported on.

In the present study, the $\text{CaGd}_2(\text{MoO}_4)_4:\text{Er}^{3+}/\text{Yb}^{3+}$ phosphors with the doping concentrations of

Er^{3+} and Yb^{3+} ($x = \text{Er}^{3+} + \text{Yb}^{3+}$, $\text{Er}^{3+} = 0.05, 0.1, 0.2$ and $\text{Yb}^{3+} = 0.2, 0.45$) were synthesized by the microwave sol-gel method, and the crystal structure refinement and UC photoluminescence properties evaluation were performed. The synthesized $\text{CaGd}_2(\text{MoO}_4)_4:\text{Er}^{3+}/\text{Yb}^{3+}$ particles were characterized by X-ray diffraction (XRD), scanning electron microscopy (SEM), and energy-dispersive X-ray spectroscopy (EDS). The spectroscopic properties were examined comparatively using photoluminescence (PL) emission and Raman spectroscopy.

2. Experimental

Appropriate stoichiometric amounts of $\text{Ca}(\text{NO}_3)_2$ (99%, Sigma-Aldrich, USA), $\text{Gd}(\text{NO}_3)_3 \cdot 6\text{H}_2\text{O}$ (99%, Sigma-Aldrich, USA), $(\text{NH}_4)_6\text{Mo}_7\text{O}_{24} \cdot 4\text{H}_2\text{O}$ (99%, Alfa Aesar, USA), $\text{Er}(\text{NO}_3)_3 \cdot 5\text{H}_2\text{O}$ (99.9%, Sigma-Aldrich, USA), $\text{Yb}(\text{NO}_3)_3 \cdot 5\text{H}_2\text{O}$ (99.9%, Sigma-Aldrich, USA), citric acid (99.5%, Daejung Chemicals, Korea), NH_4OH (A.R.), ethylene glycol (A.R.) and distilled water were used as initial reagents to prepare the $\text{CaGd}_2(\text{MoO}_4)_4$, $\text{CaGd}_{1.8}(\text{MoO}_4)_4:\text{Er}_{0.2}$, $\text{CaGd}_{1.7}(\text{MoO}_4)_4:\text{Er}_{0.1}\text{Yb}_{0.2}$ and $\text{CaGd}_{1.5}(\text{MoO}_4)_4:\text{Er}_{0.05}\text{Yb}_{0.45}$ compounds with the doping concentrations of Er^{3+} and Yb^{3+} ($\text{Er}^{3+} = 0.05, 0.1, 0.2$ and $\text{Yb}^{3+} = 0.2, 0.45$).

To prepare $\text{CaGd}_2(\text{MoO}_4)_4$, 0.4 mol% $\text{Ca}(\text{NO}_3)_2$ and 0.23 mol% $(\text{NH}_4)_6\text{Mo}_7\text{O}_{24} \cdot 4\text{H}_2\text{O}$ were dissolved in 20 mL of ethylene glycol and 80 mL of 5M NH_4OH under vigorous stirring and heating. Subsequently, 0.8 mol% $\text{Gd}(\text{NO}_3)_3 \cdot 6\text{H}_2\text{O}$ and citric acid (with a molar ratio of citric acid to total metal ions content of 2:1) were dissolved in 100 mL of distilled water under vigorous stirring and heating. Then, the solutions were mixed together under vigorous stirring and heated at 80-100°C. At the end, the highly transparent solutions were obtained and adjusted to pH = 7-8 by the NH_4OH or citric acid addition. In the second way, to prepare $\text{CaGd}_{1.8}(\text{MoO}_4)_4:\text{Er}_{0.2}$, the mixture of 0.72 mol% $\text{Gd}(\text{NO}_3)_3 \cdot 6\text{H}_2\text{O}$ and 0.08 mol% $\text{Er}(\text{NO}_3)_3 \cdot 5\text{H}_2\text{O}$ was used to create the rare earth solution. In the third way, to prepare $\text{CaGd}_{1.7}(\text{MoO}_4)_4:\text{Er}_{0.1}\text{Yb}_{0.2}$, the mixture of 0.68 mol% $\text{Gd}(\text{NO}_3)_3 \cdot 6\text{H}_2\text{O}$ and 0.04 mol% $\text{Er}(\text{NO}_3)_3 \cdot 5\text{H}_2\text{O}$ and 0.08 mol% $\text{Yb}(\text{NO}_3)_3 \cdot 5\text{H}_2\text{O}$ was used to create

the rare earth solution. In the fourth way, to prepare $\text{CaGd}_{1.5}(\text{MoO}_4)_4:\text{Er}_{0.05}\text{Yb}_{0.45}$, the rare earth containing solution was generated using 0.6 mol% $\text{Gd}(\text{NO}_3)_3 \cdot 6\text{H}_2\text{O}$ with 0.02 mol% $\text{Er}(\text{NO}_3)_3 \cdot 5\text{H}_2\text{O}$ and 0.18 mol% $\text{Yb}(\text{NO}_3)_3 \cdot 5\text{H}_2\text{O}$.

The transparent solutions were placed into a microwave oven operating at the frequency of 2.45 GHz and the maximum output-power of 1250 W for 30 min. The microwave reaction working cycle was controlled very precisely between 40 s on and 20 s off for 15 min followed by a further treatment of 30 s on and 30 s off for 15 min. Ethylene glycol was evaporated slowly at its boiling point. Ethylene glycol is a polar solvent at its boiling point of 197°C, and this solvent is a good medium for the microwave process. Respectively, if ethylene glycol is used as a solvent, the reactions proceed at the boiling point temperature. When microwave radiation is supplied to the ethylene-glycol-based solution, the components dissolved in the ethylene glycol can couple. The charged particles vibrate in the electric field interdependently when a large amount of microwave radiation is supplied to ethylene glycol, The samples were being treated with ultrasonic radiation for 10 min to produce a light yellow transparent sol. After this stage, the light yellow transparent sols were dried at 120°C in a dry oven to obtain black dried gels. The black dried gels were being ground and heat-treated at 900°C for 16 h in the air with a 100°C interval between 600-900°C. Finally, the white particles were obtained for $\text{CaGd}_2(\text{MoO}_4)_4$ with pink particles for the doped compositions.

The phase composition of the synthesized particles was evaluated using XRD (D/MAX 2200, Rigaku, Japan) with the scans over the range of $2\theta = 10-70^\circ$. The microstructure and surface morphology were observed using SEM/EDS (JSM-5600, JEOL, Japan). The PL spectra were recorded using a spectrophotometer (Perkin Elmer LS55, UK) at room temperature. Raman spectra measurements were performed using a LabRam Aramis (Horiba Jobin-Yvon, France) with the spectral resolution of 2 cm^{-1} . The 514.5-nm line of an Ar ion laser was used as an excitation source, and the power on the samples was kept at 0.5 mW level to avoid the sample decomposition.

3. Results and discussion

The XRD patterns recorded from the synthesized molybdates are shown in Fig. 1. Almost all peaks were indexed by a tetragonal unit cell in space group $I4_1/a$ with the parameters close to those of CaMoO_4 , powellite [43]. The most intensive secondary phase reflexes were detected at $2\theta \sim 26^\circ$ and $\sim 32^\circ$. Earlier, the similar impurity peaks were observed in $\text{Er}^{3+}/\text{Yb}^{3+}$ -doped CaMoO_4 phosphor at the doping concentrations of $\text{Er}^{3+}/\text{Yb}^{3+} = 0.02/0.18$ mol% [44]. It is very difficult, however, to identify the secondary phase because of a low number and low intensity of the foreign diffraction peaks. Therefore, the CaMoO_4 crystal structure was taken as a starting model for the Rietveld refinement. In the structures, the Ca^{2+} site was supposed to be occupied by a mixture of Ca^{2+} , Gd^{3+} , Er^{3+} , Yb^{3+} ions with fixed partial occupations according to the nominal chemical compositions. The refinement was stable and it gave low R -factors, and the difference Rietveld plots are shown in Fig. 1. The structural information obtained for the molybdates can be found in the Supporting Information. The defined crystal structure contains the $[\text{MoO}_4]^{2-}$ tetrahedrons coordinated by four $(\text{Ca}/\text{Gd}/\text{Er}/\text{Yb})\text{O}_8$ square antiprisms through common O ions, as shown in Fig. 2, where the structure of $\text{CaGd}_2(\text{MoO}_4)_4$ is depicted. In the $\text{CaGd}_2(\text{MoO}_4)_4:\text{Er}^{3+}/\text{Yb}^{3+}$ molybdates, the unit cell volume decreases proportionally to the integrated doping level x increase, as it is evident from Fig. 3. As it appears, the decrease seems to be due to known ionic radii relation $R(\text{Gd}^{3+}, \text{CN} = 8) = 1.053$, $R(\text{Er}^{3+}, \text{CN} = 8) = 1.004$ and $R(\text{Yb}^{3+}, \text{CN} = 8) = 0.985 \text{ \AA}$ [45], and the substitution of big Gd^{3+} ions by smaller Er^{3+} and Yb^{3+} ions is reasonably resulted in the unit cell shrinkage.

In the present study, the $\text{CaGd}_2(\text{MoO}_4)_4$ structure is defined for the first time, and it is interesting to compare this structure to those from across other known $\text{MB}_2(\text{MoO}_4)_4$ compounds. The suite of known $\text{MB}_2(\text{MoO}_4)_4$ structures is reported in Table 1. Up to now, only monoclinic and tetragonal scheelite-type structures have been found in the compounds. Previously, for the double molybdates $\text{AB}(\text{MoO}_4)_2$ (A – alkaline metals, Cu or Tl, B – trivalent rare-earth ion), it was shown that the ratio

of ionic radii R_A/R_B is a key factor governing the crystal system [56]. The $MB_2(MoO_4)_4$ compounds also belong to double molybdates but they contain alkaline-earth or bivalent rare-earth metal ions M. It is proposed to use the ionic ratio R_M/R_B for the compounds with general formula $MB_2(MoO_4)_4$. The related structural diagram is shown in Fig. 4. One can see that the monoclinic structures in the $MB_2(MoO_4)_4$ compounds are possible only at relatively high R_M/R_B ratios observed in Ba-containing crystals. This means, for example, that monoclinic structures can not form in the $CaB_2(MoO_4)_4$ crystals. In the $CaGd_2(MoO_4)_4:Er^{3+}/Yb^{3+}$ molybdates, the R_{Ca}/R_B ratio is close to 1, and these compounds can crystallize only in high symmetry space group $I4_1/a$. The situation with the symmetry of $SrB_2(MoO_4)_2$ molybdates is less predictable because the compounds, if existing, should possess boundary ratios R_{Sr}/R_B .

Thus, the microwave sol-gel route is suitable for the growth of the $CaGd_2(MoO_4)_4:Er^{3+}/Yb^{3+}$ crystalline solid solutions similarly to simple molybdates from the $CaMoO_4$ family [44, 57]. The post heat-treatment at 900°C plays an important role in the formation of a well-defined microparticle morphology. It is evident, however, that the Er^{3+}/Yb^{3+} doping level induces a great effect on the unit cell volume of the tetragonal-phase solid solutions because of a noticeably different rare-earth ion size.

The SEM images of the synthesized $CaGd_2(MoO_4)_4:Er^{3+}/Yb^{3+}$ particles are shown in Fig. 5. The samples crystallized with the formation of homogeneous partly agglomerated particles with the size of 2-10 μm . The well faceted tetragonal microcrystal forms were not found, and an irregular crystal form domination may be provided by a comparatively short synthesis time, when the equilibrium microcrystal forms were not obtained. The recorded EDS patterns and quantitative compositions of the $CaGd_{1.8}(MoO_4)_4:Er_{0.2}$ and $CaGd_{1.5}(MoO_4)_4:Er_{0.05}Yb_{0.45}$ samples are shown in Fig. 1S. Only constituent elements are found in the samples and the quantitative compositions are in good relation with nominal compositions. This result confirms the persistence of the designed chemical composition during the cyclic microwave-modified sol-gel synthesis. It is emphasized that the

microwave sol-gel process provides the energy uniformly to the bulk of the material, so that the fine particles with controlled morphology can be fabricated for a short time. The method is a cost-effective way to provide homogeneous double molybdate products with an easy scale-up potential, and it is a viable alternative for the rapid synthesis of UC particles.

The Raman spectrum recorded from $\text{CaGd}_2(\text{MoO}_4)_4$ is shown in Fig. 6, and the spectrum decomposition can be observed in Figs. 2S and 3S. About 15 narrow lines were revealed, and the total Raman line set observed in $\text{CaGd}_2(\text{MoO}_4)_4$ is shown in Table 2. The Raman spectrum of $\text{CaGd}_2(\text{MoO}_4)_4$ can be divided into two parts with a wide empty gap of 500-700 cm^{-1} that is common in the molybdates with MoO_4 tetrahedrons [3,30,31,58-62]. In the range of stretching vibrations of MoO_4 tetrahedrons (720-960 cm^{-1}) seven lines were observed. A vibrational representation for the tetragonal phase at Brillouin zone center (with respect to occupancy) is:

$$\Gamma_{\text{vibr}} = 3A_g + 6B_g + 6E_g + 6A_u + 3B_u + 6E_u \quad (1)$$

The acoustic and optic modes are:

$$\Gamma_{\text{acoustic}} = A_u + E_u \quad (2)$$

$$\Gamma_{\text{optic}} = 3A_g + 6B_g + 6E_g + 5A_u + 5E_u \quad (3)$$

The infrared and Raman active modes are:

$$\Gamma_{\text{raman}} = 3A_g + 6B_g + 6E_g \quad (4)$$

$$\Gamma_{\text{infrared}} = 5A_u + 5E_u \quad (5)$$

To calculate the $\text{CaGd}_2(\text{MoO}_4)_4$ vibrational spectrum the program package LADY was used [63]. The atomic vibration values were obtained using the modified random-element-isodisplacement model [64]. The model parameters obtained for $\text{CaGd}_2(\text{MoO}_4)_4$ are shown in Table 3. The calculated parameters of the Raman active modes are shown in Table 2 in comparison with the experimental results. The calculations show that only three and twelve Raman active modes

should appear in the spectral ranges of $>700\text{ cm}^{-1}$ and $<500\text{ cm}^{-1}$, respectively.

The strong high-wavenumber band at 903 cm^{-1} is assigned to the ν_1 symmetric stretching vibration of MoO_4 tetrahedrons [65]. The lines measured at 921 and 939 cm^{-1} correspond to Mo–O anti-symmetric stretching vibrations. The calculations show the absence of other Raman lines in the Mo–O stretching vibrations region of $>700\text{ cm}^{-1}$. The extra lines detected at 880 , 830 , 801 and 770 cm^{-1} could be assigned to impurities substituting molybdenum in the crystal structure. Such assignment is supported by the XRD data. Another possible contribution is the presence of disordered MoO_4 tetrahedrons. The ν_2 and ν_4 and bending modes of the MoO_4 groups are observed over the $250 - 450\text{ cm}^{-1}$ range. Generally, the frequency of ν_2 vibration should be lower than the frequency of ν_4 vibration [65]. For example, the line at 323 cm^{-1} corresponds to the ν_2 vibration of MoO_4 . The Raman bands at 322 and 351 cm^{-1} correspond to the mixed vibrations of MoO_4 tetrahedrons and calcium vibration along and across the c-axis of the crystal. The same behavior is observed for the Raman bands at 395 and 415 cm^{-1} , where ν_4 vibration of MoO_4 is mixed with the Ca^{2+} vibrations. The line at 211 cm^{-1} is assigned to the rotation of MoO_4 tetrahedrons along the c-axis. The calculated vibrations of gadolinium ions locate in the range of $<200\text{ cm}^{-1}$. Regrettably, this part of experimental spectrum can not be clearly decomposed.

The UC photoluminescence emission spectra of the as-prepared pure and doped $\text{CaGd}_2(\text{MoO}_4)_4$ particles excited under 980 nm at room temperature are shown in Fig. 7. The $\text{CaGd}_{1.7}(\text{MoO}_4)_4:\text{Er}_{0.1}\text{Yb}_{0.2}$ and $\text{CaGd}_{1.5}(\text{MoO}_4)_4:\text{Er}_{0.05}\text{Yb}_{0.45}$ particles exhibit a strong emission band at 525 nm and a weak emission band at 550 nm in the green region, and the bands correspond to the ${}^2\text{H}_{11/2} \rightarrow {}^4\text{I}_{15/2}$ and ${}^4\text{S}_{3/2} \rightarrow {}^4\text{I}_{15/2}$ transitions, respectively. The very weak 655-nm emission band in the red region corresponds to the ${}^4\text{F}_{9/2} \rightarrow {}^4\text{I}_{15/2}$ transition. The UC intensities in the $\text{CaGd}_2(\text{MoO}_4)_4$ and $\text{CaGd}_{1.8}(\text{MoO}_4)_4:\text{Er}_{0.2}$ have not been detected. The UC intensity of the $\text{CaGd}_{1.5}(\text{MoO}_4)_4:\text{Er}_{0.05}\text{Yb}_{0.45}$ solid solution is much higher than that of the $\text{CaGd}_{1.7}(\text{MoO}_4)_4:\text{Er}_{0.1}\text{Yb}_{0.2}$ particles. Earlier, similar results were also observed from other

Er³⁺/Yb³⁺ co-doped host matrices, which were assigned in the UC emission spectra with the green emission (${}^2\text{H}_{11/2} \rightarrow {}^4\text{I}_{15/2}$ and ${}^4\text{S}_{3/2} \rightarrow {}^4\text{I}_{15/2}$ transitions) and the red emission (${}^4\text{F}_{9/2} \rightarrow {}^4\text{I}_{15/2}$ transition) intensities [27, 34, 44, 66, 67]. The Er³⁺/Yb³⁺ doping amounts greatly influenced the morphological features of the particles and their UC fluorescence intensity.

The Yb³⁺ ion sensitizer in the Er³⁺/Yb³⁺ co-doped UC phosphors can be efficiently excited by the energy of the incident light source, which transfers this energy to the activator, where radiation can be emitted. The Er³⁺ ion activator is the luminescence center in UC particles, and the sensitizer enhances the UC luminescence efficiency due to the energy matching of the gap between the ${}^2\text{F}_{7/2}$ and the ${}^2\text{F}_{5/2}$ of Yb³⁺. The schematic energy level diagrams of Er³⁺ ions (activator) and Yb³⁺ ions (sensitizer) in the CaGd₂(MoO₄)₄:Er³⁺/Yb³⁺ samples and the UC mechanisms accounting for the green and red emissions at the 980 nm laser excitation are shown in Fig. 8. The UC emissions are generated through multiple processes of ground state absorption (GSA) and energy transfer (ET). For the green emissions, under the excitation of 980 nm, the Yb³⁺ ion sensitizer is excited from the ground ${}^2\text{F}_{7/2}$ state to the excited ${}^2\text{F}_{5/2}$ state through the GSA process, transfers the energy to the excited Er³⁺ ions and promotes it from the ${}^4\text{I}_{15/2}$ to the ${}^4\text{I}_{11/2}$ by the ET process of ${}^4\text{I}_{15/2}(\text{Er}^{3+}) + {}^2\text{F}_{5/2}(\text{Yb}^{3+}) \rightarrow {}^4\text{I}_{11/2}(\text{Er}^{3+}) + {}^2\text{F}_{7/2}(\text{Yb}^{3+})$. Another Yb³⁺ ion at the ${}^2\text{F}_{5/2}$ level transfers the energy to the excited Er³⁺ ion, and then transmits further the energy from the ${}^4\text{I}_{11/2}$ to the higher ${}^4\text{F}_{7/2}$ level by another ET process of ${}^4\text{I}_{11/2}(\text{Er}^{3+}) + {}^2\text{F}_{5/2}(\text{Yb}^{3+}) \rightarrow {}^4\text{F}_{7/2}(\text{Er}^{3+}) + {}^2\text{F}_{7/2}(\text{Yb}^{3+})$, which are for the population of the different levels in Er³⁺. The populated ${}^4\text{F}_{7/2}$ level relaxes rapidly and non-radiatively to the next lower ${}^2\text{H}_{11/2}$ and ${}^4\text{S}_{3/2}$ levels in Er³⁺ because of the short lifetime of the ${}^4\text{F}_{7/2}$ level. Then, the radiative transitions of ${}^2\text{H}_{11/2} \rightarrow {}^4\text{I}_{15/2}$ and ${}^4\text{S}_{3/2} \rightarrow {}^4\text{I}_{15/2}$ processes can produce green emission at 525 and 550 nm. It is noted that the green upconversion luminescence can be induced by a two-photon process [27, 66]. For the red emission, the ${}^4\text{F}_{9/2}$ level is populated by non-radiative relaxation from the ${}^4\text{S}_{3/2}$ to the ${}^4\text{F}_{9/2}$ level and the second ET from the ${}^4\text{I}_{13/2}$ to the ${}^4\text{F}_{9/2}$ level in Er³⁺. Finally, the ${}^4\text{F}_{9/2}$ level relaxes radiatively to the ground state at the ${}^4\text{I}_{15/2}$ level, and red emission is

released at 655 nm [67, 68]. The strong 525-nm and 550-nm emission bands in the green region, as shown in Fig. 7, are assigned to the ${}^2\text{H}_{11/2} \rightarrow {}^4\text{I}_{15/2}$ and ${}^4\text{S}_{3/2} \rightarrow {}^4\text{I}_{15/2}$ transitions of the Er^{3+} ions, respectively, while the weak 655-nm emission band in the red region is assigned to the ${}^4\text{F}_{9/2} \rightarrow {}^4\text{I}_{15/2}$ transition. The much higher intensity of the ${}^2\text{H}_{11/2} \rightarrow {}^4\text{I}_{15/2}$ transition in comparison with that of the ${}^4\text{S}_{3/2} \rightarrow {}^4\text{I}_{15/2}$ transition in Fig. 7 may be induced with the concentration quenching effect by the energy transfer between the nearest Er^{3+} and Yb^{3+} ions and the interactions between the doping ions in the host matrix [27, 44]. It means that the green band induced by the ${}^2\text{H}_{11/2} \rightarrow {}^4\text{I}_{15/2}$ transitions is assumed to be more easily quenched than that of the ${}^4\text{S}_{3/2} \rightarrow {}^4\text{I}_{15/2}$ transition by the non-radiative relaxation in the case of the $\text{CaGd}_2(\text{MoO}_4)_4$ host matrix.

The emission spectra of the Er-containing samples of $\text{CaGd}_{1.8}(\text{MoO}_4)_4:\text{Er}_{0.2}$ (CGM:Er), $\text{CaGd}_{1.7}(\text{MoO}_4)_4:\text{Er}_{0.1}\text{Yb}_{0.2}$ (CGM:ErYb) and $\text{CaGd}_{1.5}(\text{MoO}_4)_4:\text{Er}_{0.05}\text{Yb}_{0.45}$ (CGM:ErYb#) are shown in Fig. 4S. All spectra were obtained under the excitation by a 514.5-nm line of an Ar ion laser at 0.5 mW on the samples. The spectrum of the undoped $\text{CaGd}_2(\text{MoO}_4)_4$ sample is well interpreted in terms of Raman scattering, as described above. However, the shape of spectra recorded from the samples doped with Er strongly differ from that of undoped sample. At the same time, the shapes of the spectra of all Er-containing samples are very similar with each other and weakly vary with the erbium content as well as with the presence of a large ytterbium content. The wavelength region occupied by the spectra obtained in the erbium-doped samples excited at 514.5 nm fairly coincides with the UC luminescence observed for them using excitation at 980 nm, as well as with the well-known erbium luminescence in many other hosts (see, e.g. [69]). However, the relative luminescence intensity at ${}^2\text{H}_{11/2} \rightarrow {}^4\text{I}_{15/2}$ and ${}^4\text{S}_{3/2} \rightarrow {}^4\text{I}_{15/2}$ transitions under excitation at 514.5 nm differs from the case of UC luminescence. This is understandable since, in case of UC, predominantly the ${}^2\text{F}_{7/2}$ state is excited, while under 514.5 nm irradiation the excitation wavelength falls into the high-energy wing of ${}^4\text{I}_{15/2} \rightarrow {}^2\text{H}_{11/2}$ transition. This leads to the difference in populations of ${}^2\text{H}_{11/2}$ and ${}^4\text{S}_{3/2}$ in cases of UC and direct 514.5 nm excitation. The strongest

luminescence due to both ${}^2\text{H}_{11/2} \rightarrow {}^4\text{I}_{15/2}$ and ${}^4\text{S}_{3/2} \rightarrow {}^4\text{I}_{15/2}$ transitions is observed in the sample with 10 at. % of erbium. However, integral ${}^2\text{H}_{11/2} \rightarrow {}^4\text{I}_{15/2}$ luminescence from the sample with 20 at. % of erbium is weaker than that from the sample with 5 at.%. Oppositely, for the ${}^4\text{S}_{3/2} \rightarrow {}^4\text{I}_{15/2}$ transition, the luminescence from the sample with 20 at. % of erbium is stronger than that from the sample with 5 at.%. Consecutively, the influence of concentration quenching for both transitions is established approximately nearby the 10% erbium content, but it is slightly weaker for the ${}^4\text{S}_{3/2} \rightarrow {}^4\text{I}_{15/2}$ transition. Thus, it can be concluded that the spectra shown in Fig. 4S are not Raman and relate to emission due to electron transitions at the Er^{3+} levels.

4. Conclusions

UC $\text{CaGd}_2(\text{MoO}_4)_4:\text{Er}^{3+}/\text{Yb}^{3+}$ phosphors with the doping concentrations of Er^{3+} and Yb^{3+} were successfully synthesized by the microwave sol-gel method. The synthesized particles, being formed after the heat-treatment at 900°C for 16 h, showed a well crystallized morphology with the particle sizes of 2-10 μm . Under the excitation at 980 nm, $\text{CaGd}_{1.7}(\text{MoO}_4)_4:\text{Er}_{0.1}\text{Yb}_{0.2}$ and $\text{CaGd}_{1.5}(\text{MoO}_4)_4:\text{Er}_{0.05}\text{Yb}_{0.45}$ particles exhibited a strong 525-nm emission band and a weak 550-nm emission band in the green region, which were assigned to the ${}^2\text{H}_{11/2} \rightarrow {}^4\text{I}_{15/2}$ and ${}^4\text{S}_{3/2} \rightarrow {}^4\text{I}_{15/2}$ transitions, respectively, while a very weak 655-nm emission band in the red region was assigned to the ${}^4\text{F}_{9/2} \rightarrow {}^4\text{I}_{15/2}$ transition. The UC intensity of $\text{CaGd}_{1.5}(\text{MoO}_4)_4:\text{Er}_{0.05}\text{Yb}_{0.45}$ particles was much higher than that of the $\text{CaGd}_{1.7}(\text{MoO}_4)_4:\text{Er}_{0.1}\text{Yb}_{0.2}$ particles. The experimental Raman spectra of undoped $\text{CaGd}_{1.7}(\text{MoO}_4)_4$ are in good agreement with the calculations. 514.5 nm excited spectra of the samples doped with Er and Yb are dominated by Er luminescence. Concentration quenching of the erbium luminescence at the ${}^2\text{H}_{11/2} \rightarrow {}^4\text{I}_{15/2}$ and ${}^4\text{S}_{3/2} \rightarrow {}^4\text{I}_{15/2}$ transitions in the $\text{CaGd}_2(\text{MoO}_4)_4:\text{Er}^{3+}/\text{Yb}^{3+}$ crystal structure was established approximately at the 10 at.% doping level.

Acknowledgements

This study was supported by the Basic Science Research Program through the National Research Foundation of Korea (NRF) funded by the Ministry of Science, ICT & Future Planning (2014-046024). VVA and ASA are partially supported by the Ministry of Education and Science of the Russian Federation.

References

- [1] Chun Che Lin and Ru-Shi Liu, Advances in Phosphors for Light-emitting Diodes, *J. Phys. Chem. Lett.* 2 (2011) 1268-1277.
- [1] Nathan C. George, Kristin A. Denault, Ram Seshadri, Phosphors for solid-state white lighting, *Annu. Rev. Mater. Res.* 43 (2013) 481–501.
- [2] Zhiguo Xia, Yuanyuan Zhang, Maxim S. Molokeev, Victor V. Atuchin, Structural and luminescence properties of yellow-emitting $\text{NaScSi}_2\text{O}_6:\text{Eu}^{2+}$ phosphors: Eu^{2+} site preference analysis and generation of red emission by codoping Mn^{2+} for white-light-emitting diode applications, *J. Phys. Chem. C* 117 (2013) 20847-20854.
- [3] V.V. Atuchin, O.D. Chimitova, S.V. Adichtchev, B.G. Bazarov, T.A. Gavrilova, M.S. Molokeev, N.V. Surovtsev, Zh.G. Bazarova, Synthesis, structural and vibrational properties of microcrystalline $\beta\text{-RbSm}(\text{MoO}_4)_2$, *Mater. Lett.* 106 (2013) 26-29.
- [4] Zhiguo Xia, Yuanyuan Zhang, Maxim S. Molokeev, Victor V. Atuchin and Yi Luo, Linear structural evolution induced tunable photoluminescence in clinopyroxene solid-solution phosphors, *Sci. Reports* 3 (2013) 3310.
- [5] Chien-Hao Huang, Yuan-Tai Lai, Ting-Shan Chan, Yao-Tsung Yeh, Wei-Ren Liu, A novel green-emitting $\text{SrCaSiAl}_2\text{O}_7:\text{Eu}^{2+}$ phosphor for white LEDs, *RSC Adv.* 4 (2014) 7811-7817.
- [6] R.J. Yu, S.L. Zhong, N. Xue, H.J. Li, H.L. Ma, Synthesis, structure, and peculiar green emission of $\text{NaBaBO}_3:\text{Ce}^{3+}$ phosphors, *Dalton Trans.* 43 (28) (2014) 10969-10976.
- [7] Haipeng Ji, Zhaohui Huang, Zhiguo Xia, Maxim S. Molokeev, Victor V. Atuchin, Minghao Fang, Saifang Huang, New yellow-emitting whitlockite-type structure $\text{Sr}_{1.75}\text{Ca}_{1.25}(\text{PO}_4)_2:\text{Eu}^{2+}$ phosphor for near-UV pumped white light-emitting devices, *Inorg. Chem.* 53 (10) (2014) 5129-5135.
- [8] Mengfei Zhang, Yujun Liang, Rui Tang, Dongyan Yu, Miaohui Tong, Qiang Wang, Yingli Zhu, Xingya Wu and Guogang Li, Highly efficient $\text{Sr}_3\text{Y}_2(\text{Si}_3\text{O}_9)_2:\text{Ce}^{3+},\text{Tb}^{3+}/\text{Mn}^{2+}/\text{Eu}^{2+}$ phosphors for

- white LEDs: structure refinement, color tuning and energy transfer, *RSC Adv.* 4 (2014) 40626-40637.
- [9] V.V. Atuchin, A.S. Aleksandrovsky, O.D. Chimitova, A.S. Krylov, M.S. Molokeev, B.G. Bazarov, J.G. Bazarova, Zhiguo Xia, Synthesis and spectroscopic properties of multiferroic β' - $\text{Tb}_2(\text{MoO}_4)_3$, *Opt. Mater.* 36 (10) (2014) 156-159.
- [10] M. Haase, H. Schäfer, Upconverting nanoparticles, *Angew. Chem. Int. Ed.* 50 (2011) 5808-5829.
- [11] C.S. Lim, Preparation of $\text{CaLa}_2(\text{MoO}_4)_4:\text{Er}^{3+}/\text{Yb}^{3+}$ phosphors and the upconversion of their photoluminescence properties, *Mater. Res. Bull.* 60 (2014) 537-542.
- [12] A.I. Orlova, S.N. Pleskova, N.V. Malanina, A.N. Shushunov, E.N. Gorshkova, E.E. Pudovkina, O.N. Gorshkov, $\text{Ca}_3(\text{PO}_4)_2:\text{Er}^{3+}, \text{Yb}^{3+}$: An upconversion phosphor for in vivo imaging, *Inorg. Mater.* 49 (7) (2013) 696-700.
- [13] Yang Zhang, Jianhua Hao, Color-tunable upconversion luminescence of Yb^{3+} , Er^{3+} , and Tm^{3+} tri-doped ferroelectric BaTiO_3 materials, *J. Appl. Phys.* 113 (2013) 184112.
- [14] Hyeon Mi Noh, Hyun Kyoung Yang, Byung Kee Moon, Byung Chun Choi, Jung Hyun Jeong, Haeyoung Choi, Jung Hwan Kim, Concentration enhanced upconversion luminescence in $\text{ZrO}_2:\text{Ho}^{3+}, \text{Yb}^{3+}$ nanophosphors, *J. Nanosci. Nanotech.* 13 (2013) 4006-4009.
- [15] Lin Li, Chongfeng Guo, Sha Jiang, Dinesh K. Agrawal, Ting Li, Green up-conversion luminescence of $\text{Yb}^{3+}-\text{Er}^{3+}$ co-doped $\text{CaLa}_2\text{ZnO}_5$ for optically temperature sensing, *RSC Adv.* 4 (2014) 6391-6396.
- [16] C.S. Lim, Upconversion photoluminescence properties of $\text{SrY}_2(\text{MoO}_4)_4:\text{Er}^{3+}/\text{Yb}^{3+}$ phosphors, *Infr. Phys. Tech.* 67, (2014) 371-376.
- [17] A. Pandey, S. Som, V. Kumar, V. Kumar, K. Kumar, V.K. Rai, H.C. Swart, Enhanced upconversion and temperature sensing study of $\text{Er}^{3+}-\text{Yb}^{3+}$ codoped tungsten-tellurite glass, *Sens. Actuat. B Chem.* 202 (2014) 1305-1312.

- [18] M. Wang, G. Abbineni, A. Clevenger, C. Mao, S. Xu, Upconversion nanoparticles: synthesis, surface modification and biological applications, *Nanomedicine: Nanotech. Biol. Med.* 7 (2011) 710-729.
- [19] Y.J. Chen, H.M. Zhu, Y.F. Lin, X.H. Gong, Z.D. Luo, Y.D. Huang, Efficient diode-pumped continuous-wave monolithic 1.9 μm micro-laser based on $\text{Tm}^{3+}:\text{BaGd}_2(\text{MoO}_4)_4$ cleaved plate, *Opt. Mater.* 35 (2013) 1422-1425.
- [20] M. Lin, Y. Zho, S. Wang, M. Liu, Z. Duan, Y. Chen, F. Li, F. Xu, T. Lu, *Bio. Adv.* 30 (2012) 1551-1561.
- [21] J. Liao, D. Zhou, B. Yang, R. Liu, Q. Zhang, Q. Zhou, Sol-gel preparation and photoluminescence properties of $\text{CaLa}_2(\text{MoO}_4)_4:\text{Eu}^{3+}$ phosphors, *J. Lumin.* 134 (2013) 533-538.
- [22] J. Sun, Y. Lan, Z. Xia, H. Du, Sol-gel synthesis and green upconversion luminescence in $\text{BaGd}_2(\text{MoO}_4)_4:\text{Yb}^{3+},\text{Er}^{3+}$ phosphors, *Opt. Mater.* 33 (2011) 576-581.
- [23] C. Guo, H. K. Yang, J.H. Jeong, Preparation and luminescent properties of phosphor $\text{MGd}_2(\text{MoO}_4)_4:\text{Eu}^{3+}$ (M=Ca, Sr and Ba), *J. Lumin.* 130 (2010) 1390-1393.
- [24] J. Sun, J. Xian, H. Du, Hydrothermal synthesis of $\text{BaYF}_5:\text{Yb}^{3+}/\text{Er}^{3+}$ upconversion luminescence submicrospheres by a surfactant-free aqueous solution route, *J. Phys. Chem. Solids* 72 (2011) 207-213.
- [25] V.K. Komarala, Y. Wang, M. Xiao, Nonlinear optical properties of $\text{Er}^{3+}/\text{Yb}^{3+}$ -doped NaYF_4 nanocrystals, *Chem. Phys. Lett.* 490 (2010) 189-193.
- [26] J. Sun, J. Xian, Z. Xia, H. Du, Synthesis of well oil-dispersible $\text{BaYF}_5:\text{Yb}^{3+}/\text{Er}^{3+}$ nanocrystals with green upconversion fluorescence, *J. Rare Earths* 28 (Spec. Issue, Dec.) (2010) 219-221.
- [27] H. Du, Y. Lan, Z. Xia, J. Sun, Synthesis and upconversion luminescence properties of $\text{Yb}^{3+}/\text{Er}^{3+}$ codoped $\text{BaGd}_2(\text{MoO}_4)_4$ powder, *Mater. Res. Bull.* 44 (2009) 1660-1662.
- [28] L.X. Pang, H. Liu, D. Zhou, G.B. Sun, W.B. Qin, W.G. Liu, Microwave dielectric ceramic with intrinsic low firing temperature: $\text{BaLa}_2(\text{MoO}_4)_4$, *Mater. Lett.* 72 (2012) 128-130.

- [29] M. Haque, D.K. Kim, Luminescent properties of Eu^{3+} activated $\text{MLa}_2(\text{MoO}_4)_4$ based (M = Ba, Sr and Ca) novel red-emitting phosphors, *Mater. Lett.* 63 (2009) 793-796.
- [30] V.V. Atuchin, O.D. Chimitova, T.A. Gavrilova, M.S. Molokeev, Sung-Jin Kim, N.S. Surovtsev, B.G. Bazarov, Synthesis, structural and vibrational properties of microcrystalline $\text{RbNd}(\text{MoO}_4)_2$, *J. Cryst. Growth* 318 (2011) 683-686.
- [31] V.V. Atuchin, V.G. Grossman, S.V. Adichtchev, N.V. Surovtsev, T.A. Gavrilova, B.G. Bazarov, Structural and vibrational properties of microcrystalline $\text{TlM}(\text{MoO}_4)_2$ (M = Nd, Pr) molybdates, *Opt. Mater.* 34 (2012) 812-816.
- [32] L. Qin, Y. Huang, T. Tsuboi, H.J. Seo, The red-emitting phosphors of Eu^{3+} -activated $\text{MR}_2(\text{MoO}_4)_4$ (M = Ba, Sr, Ca; R = La^{3+} , Gd^{3+} , Y^{3+}) for light emitting diodes, *Mater. Res. Bull.* 47 (2012) 4498-4502.
- [33] Y.L. Yang, X.M. Li, W.L. Feng, W.L. Li, C.Y. Tao, Co-precipitation synthesis and photoluminescence properties of $(\text{Ca}_{1-x-y}\text{Ln}_y)\text{MoO}_4: x\text{Eu}^{3+}$ (Ln = Y, Gd) red phosphors *J. Alloys Compd.* 505 (2010) 239-242.
- [34] Y. Tian, B. Chen, B. Tian, R. Hua, J. Sun, L. Cheng, H. Zhong, X. Li, J. Zhang, Y. Zheng, T. Yu, L. Huang, Q. Meng, Concentration-dependent luminescence and energy transfer of flower-like $\text{Y}_2(\text{MoO}_4)_3:\text{Dy}^{3+}$ phosphor, *J. Alloy Compd.* 509 (2011) 6096-6102.
- [35] Y. Huang, L. Zhou, Z. Tang, Self-assembled 3D flower-like $\text{NaY}(\text{MoO}_4)_2:\text{Eu}^{3+}$ microarchitectures: Hydrothermal synthesis, formation mechanism and luminescence properties, *Opt. Mater.* 33 (2011) 777-782.
- [36] Y. Tian, B. Chen, B. Tian, J. Sun, X. Li, J. Zhang, L. Cheng, H. Zhong, H. Zhong, Q. Meng, R. Hua, Ionic liquid-assisted hydrothermal synthesis of dendrite-like $\text{NaY}(\text{MoO}_4)_2:\text{Tb}^{3+}$ phosphor, *Physica B* 407 (2012) 2556-2559.

- [37] Z. Wang, H. Liang, L. Zhou, J. Wang, M. Gong, Q. Su, NaEu_{0.96}Sm_{0.04}(MoO₄)₂ as a promising red-emitting phosphor for LED solid-state lighting prepared by the Pechini process, *J. Lumin.* 128 (2008) 147-154.
- [38] Q. Chen, L. Qin, Z. Feng, R. Ge, X. Zhao, H. Xu, Upconversion luminescence of KGd(MoO₄)₂:Er³⁺, Yb³⁺ powder prepared by Pechini method, *J. Rare Earths*, 29 (2011) 843-848.
- [39] X. Shen, L. Li, F. He, X. Meng, F. Sing, Effects of doped-Li⁺ and -Eu³⁺ ions content on structure and luminescent properties of Li_xSr_{1-2x}(MoO₄):Eu³⁺_x red-emitting phosphors for white LEDs, *Mater. Chem. Phys.* 132 (2012) 471-475.
- [40] J. Zhang, X. Wang, X. Zhang, X. Zhao, X. Liu, L. Peng, Microwave synthesis of NaLa(MoO₄)₂ microcrystals and their near-infrared luminescent properties with lanthanide ion doping (Er³⁺, Nd³⁺, Yb³⁺), *Inorg. Chem. Commun.* 14 (2011) 1723-1727.
- [41] S. Das, A.K. Mukhopadhyay, S. Datta, D. Basu, Prospects of microwave processing: An overview, *Bull. Mater. Sci.* 32 (2009) 1-13.
- [42] T. Thongtem, A. Phuruangrat, S. Thongtem, Microwave-assisted synthesis and characterization of SrMoO₄ and SrWO₄ nanocrystals, *J. Nanopart. Res.* 12 (2010) 2287-2294.
- [43] V.B. Aleksandrov, L.V. Gorbatiy, V.V. Ilyukhin, *Kristallografiya*, 13, 512 (1968).
- [44] C.S. Lim, Cyclic MAM synthesis and upconversion photoluminescence properties of CaMoO₄:Er³⁺/Yb³⁺ particles, *Mater. Res. Bull.* 47 (2012) 4220-4225.
- [45] R.D. Shannon, *Acta Cryst. A*, 32, 751 (1976).
- [46] S. Gallinat. Beispiele fuer partielle und totale Defekte im Ba' Ln₂Mo₄O₁₆-Typ: BaCu_{0.41}' _{0.59}Pr₂Mo₄O₁₆ und Ba' Yb₂Mo₄O₁₆, *Z. Naturforsch. B: Chem. Sci.* 51 (1996) 85-89.
- [47] I.I. Kiseleva, M.I. Sirota, R.P. Ozerov, T.P. Balakireva, A.A. Maier. Barium-lanthanide double molybdates BaLn₂(MoO₄)₄. II. Crystal structure of BaNd₂(MoO₄)₄, *Kristallografiya* 24 (1979) 1277-1279.

- [48] L.S. Cavalcante, J.C. Sczancoski, R.L. Tranquilin, M.R. Joya, P.S. Pizani, J.A. Varela, E. Longo, BaMoO₄ powders processed in domestic microwave-hydrothermal: synthesis, characterization and photoluminescence at room temperature, *J. Phys. Chem. Solids* 69 (2008) 2674-2680.
- [49] L. Vegard, A. Refsum, The structure of crystals belonging to the scheelite group. *Skrifter utgitt av det Norske Videnskaps-Akademi i Oslo 1: Matematisk-Naturvidenskapelig Klasse* 1927 (2), (1927), 1-1.
- [50] E. Guermen, E. Daniels, J.S. King, Crystal structure refinement of SrMoO₄, SrWO₄, CaMoO₄, and BaWO₄ by neutron diffraction, *J. Chem. Phys.* 55 (1971) 1093-1097.
- [51] P. Gall, P. Gougeon, P. The scheelite-type europium molybdate Eu_{0.96}MoO₄. *Acta Cryst. E* 62 (2006) i120-i121.
- [52] A.V. Chichagov, L.N. Dem'yanets, V.V. Ilyukhin, N.V. Belov, Synthesis and crystal structure of cadmium molybdate (CdMoO₄), *Kristallografiya* 11 (1966) 686-689.
- [53] T. Schustereit, T. Schleid, I. Hartenbach, The defect scheelite-type lanthanum(III) ortho-oxidomolybdate(VI) La_{0.667}[MoO₄], *Acta Cryst. E* 69 (2) (2013) i7-i7.
- [54] T. Schustereit, S.L. Mueller, T. Schleid, I. Hartenbach, Defect scheelite-type lanthanoid(III) ortho-oxomolybdates(VI) Ln_{0.667}(MoO₄) (Ln = Ce, Pr, Nd and Sm) and their relationship to zircon and the (Na Tl)-type structure, *Crystals* 2011 (1) (2011), 244-253.
- [55] A. Tabuteau, M. Pages. Etude cristallographique du molybdate et du tungstate d'americium(III): alpha-Am₂(MoO₄)₃, alpha-Am₂(WO₄)₃, *J. Solid State Chem.* 26 (1978) 153-158.
- [56] O.D. Chimitova, V.V. Atuchin, B.G. Bazarov, M.S. Molokeyev, Zh.G. Bazarova, The formation and structural parameters of new double molybdates RbLn(MoO₄)₂ (Ln = Pr, Nd, Sm, Eu), *Proc. SPIE* 8771 (2013) 87711A.

- [57] V. Thangadurai, C. Knittlmayer, W. Weppner, Metathetic room temperature preparation and characterization of scheelite-type ABO_4 ($A = Ca, Sr, Ba, Pb; B = Mo, W$) powders, *Mater. Sci. Eng. B* 106 (2004) 228-233.
- [58] J. Hanuza, L. Macalik, K. Hermanowicz, Vibrational properties of $KLn(MoO_4)_2$ crystals for light rare earth ions from lanthanum to terbium, *J. Mol. Struct.* 319 (1994) 17-30.
- [59] L. Macalik, Comparison of the spectroscopic and crystallographic data of Tm^{3+} in the different hosts: $KLn(MoO_4)_2$ where $Ln = Y, La, Lu$ and $M = Mo, W$, *J. Alloys Compd.* 341 (2002) 226-232.
- [60] V. Dmitriev, V. Sinitsyn, R. Dilanian, D. Machon, A. Kuznetsov, E. Ponyatovsky, G. Lucazeau, H.P. Weber, In situ pressure-induced solid-state amorphization in $Sm_2(MoO_4)_3$, $Eu_2(MoO_4)_3$ and $Gd_2(MoO_4)_3$ crystals: chemical decomposition scenario, *J. Phys. Chem. Solids* 64 (2003) 307-312.
- [61] B.G. Bazarov, O.D. Chimitova, R.F. Klevtsova, Yu.L. Tushinova, L.A. Glinskaya, Z.G. Bazarova, Crystal structure of a new ternary molybdate in the Rb_2MoO_4 - $Eu_2(MoO_4)_3$ - $Hf(MoO_4)_2$ system, *J. Struct. Chem.* 49 (1) (2008) 53-57.
- [62] V.V. Atuchin, A.S. Aleksandrovsky, O.D. Chimitova, T.A. Gavrilova, A. S. Krylov, M.S. Molokeev, A.S. Oreshonkov, B.G. Bazarov, and J.G. Bazarova, Synthesis and spectroscopic properties of monoclinic α - $Eu_2(MoO_4)_3$, *J. Phys. Chem. C* 118 (2014) 15404–15411.
- [63] M.B. Smirnov, V.Yu. Kazimirov, LADY: software for lattice dynamics simulations. (JINR communications), E 14-2001-159, 2001.
- [64] I.F. Chang and S.S. Mitra, Application of a modified random-element-isodisplacement model to long-wavelength optic phonons of mixed crystals, *Phys. Rev.* 172 (3) (1968) 924 – 933.
- [65] K. Nakamoto, *Infrared and Raman spectra of inorganic and coordination compounds* (6th edn), Wiley, New York etc., 2009.

- [66] W. Lu, L. Cheng, J. Sun, H. Zhong, X. Li, Y. Tian, J. Wan, Y. Zheng, L. Huang, T. Yu, H. Yu, B. Chen, The concentration effect of upconversion luminescence properties in $\text{Er}^{3+}/\text{Yb}^{3+}$ -codoped $\text{Y}_2(\text{MoO}_4)_3$ phosphors, *Physica B* 405 (2010) 3284-3288.
- [67] J. Sun, B. Sue, H. Du, Synthesis and luminescence properties of $\text{Gd}_6\text{MoO}_{12}:\text{Yb}^{3+}$, Er^{3+} phosphor with enhanced photoluminescence by Li^+ doping, *Infr. Phys. Tech.* 60 (2013) 10-14.
- [68] Q. Sun, X. Chen, Z. Liu, F. Wang, Z. Jiang, C. Wang, Enhancement of the upconversion luminescence intensity in Er^{3+} doped BaTiO_3 nanocrystals by codoping with Li^+ ions, *J. Alloys Compd.* 509 (2012) 5336-5340.
- [69] A.V. Malakhovskii, T.V. Kutsak, A.L. Sukhachev, A.S. Aleksandrovsky, A.S. Krylov, I.A. Gudim, M.S. Molokeevev, Spectroscopic properties of $\text{ErAl}_3(\text{BO}_3)_4$ single crystal, *Chem. Phys.* 428 (2014) 137-143.

Table 1. Space group and big ion radii ratio for the $MB_2(MoO_4)_4$ compounds

Compound	Space group	R_M/R_B	Reference
$BaYb_2(MoO_4)_4$	$C2/c$	1.442	[46]
$BaNd_2(MoO_4)_4$	$C2/c$	1.280	[47]
$CaGd_{1.5}Er_{0.05}Yb_{0.45}(MoO_4)_4$	$I4_1/a$	1.081	This study
$CaGd_{1.7}Er_{0.1}Yb_{0.2}(MoO_4)_4$	$I4_1/a$	1.073	This study
$CaGd_{1.8}Er_{0.2}(MoO_4)_4$	$I4_1/a$	1.069	This study
$CaGd_2(MoO_4)_4$	$I4_1/a$	1.064	This study
$Ba_4(MoO_4)_4$	$I4_1/a$	1	[48]
$Pb_4(MoO_4)_4$	$I4_1/a$	1	[49]
$Sr_4(MoO_4)_4$	$I4_1/a$	1	[50]
$Ca_4(MoO_4)_4$	$I4_1/a$	1	[50]
$Eu_4(MoO_4)_4$	$I4_1/a$	1	[51]
$Cd_4(MoO_4)_4$	$I4_1/a$	1	[52]
$La_{2.667}(MoO_4)_4$	$I4_1/a$	1	[53]
$Ce_{2.667}(MoO_4)_4$	$I4_1/a$	1	[54]
$Pr_{2.667}(MoO_4)_4$	$I4_1/a$	1	[54]
$Nd_{2.667}(MoO_4)_4$	$I4_1/a$	1	[54]
$Sm_{2.667}(MoO_4)_4$	$I4_1/a$	1	[54]
$Am_{2.667}(MoO_4)_4$	$I4_1/a$	1	[55]

Table 2. Calculated and experimental relative magnitude (I), wavenumber and full width at half maximum (FWHM) of the Raman lines

Number	Symmetry type	ω , cm^{-1} (calc.)	I (exp.)	ω , cm^{-1} (exp.)	Γ (FWHM), cm^{-1}
1	E_g	960	16	939.6	17.3
2	B_g	958	27	921.4	19.25
3	A_g	903	100	903.4	20.23
			59	880.8	48.09
			27	830.8	43.6
			9	801.2	28.16
			20	770.3	43.18
4	E_g	426	12	415	28.2
5	B_g	391	37	395	18.6
6	B_g	351	21	352	30.2
			40	340	17.0
7	E_g	322	93	323	12.5
8	A_g	315	19	320	35.6
9	B_g	266	0.1	275	13.6
10	E_g	252			
11	A_g	238	9	211	23.81
12	B_g	152			
13	E_g	136			
14	E_g	84			
15	B_g	73			

Table 3. Parameters of the interatomic interaction potential

Interaction	λ , aJ/Å ²	ρ , Å
Ca – O	520.17	0.4134
Gd – O	325.17	0.4084
Mo – O	560.17	0.3834
O – O	250.17	0.3834

Figure Captions

Fig. 1. X-ray diffraction patterns of the synthesized (a) $\text{CaGd}_2(\text{MoO}_4)_4$, (b) $\text{CaGd}_{1.8}(\text{MoO}_4)_4:\text{Er}_{0.2}$, (c) $\text{CaGd}_{1.7}(\text{MoO}_4)_4:\text{Er}_{0.1}\text{Yb}_{0.2}$ and (d) $\text{CaGd}_{1.5}(\text{MoO}_4)_4:\text{Er}_{0.05}\text{Yb}_{0.45}$ particles.

Fig. 2. A crystal structure of $\text{CaGd}_2(\text{MoO}_4)_4$. The unit cell is outlined. Lone atoms are omitted for clarity.

Fig. 3. Dependence of the unit cell volume on x in the $\text{CaGd}_2(\text{MoO}_4)_4:\text{Er}^{3+}/\text{Yb}^{3+}$ crystals.

Fig. 4. A symmetry diagram of the known $\text{AB}_2(\text{MoO}_4)_4$ molybdates.

Fig. 5. Scanning electron microscopy images of the synthesized (a) $\text{CaGd}_2(\text{MoO}_4)_4$, (b) $\text{CaGd}_{1.8}(\text{MoO}_4)_4:\text{Er}_{0.2}$, (c) $\text{CaGd}_{1.7}(\text{MoO}_4)_4:\text{Er}_{0.1}\text{Yb}_{0.2}$ and (d) $\text{CaGd}_{1.5}(\text{MoO}_4)_4:\text{Er}_{0.05}\text{Yb}_{0.45}$ particles.

Fig. 6. The Raman spectrum of $\text{CaGd}_2(\text{MoO}_4)_4$.

Fig. 7. The upconversion photoluminescence emission spectra of (a) $\text{CaGd}_2(\text{MoO}_4)_4$, (b) $\text{CaGd}_{1.8}(\text{MoO}_4)_4:\text{Er}_{0.2}$, (c) $\text{CaGd}_{1.7}(\text{MoO}_4)_4:\text{Er}_{0.1}\text{Yb}_{0.2}$ and (d) $\text{CaGd}_{1.5}(\text{MoO}_4)_4:\text{Er}_{0.05}\text{Yb}_{0.45}$ particles excited under 980 nm at room temperature.

Fig. 8. Schematic energy level diagrams of Er^{3+} ions (activator) and Yb^{3+} ions (sensitizer) in the as-prepared $\text{CaGd}_2(\text{MoO}_4)_4:\text{Er}^{3+}/\text{Yb}^{3+}$ system and the upconversion mechanisms accounting for the green and red emissions under 980-nm laser excitation.

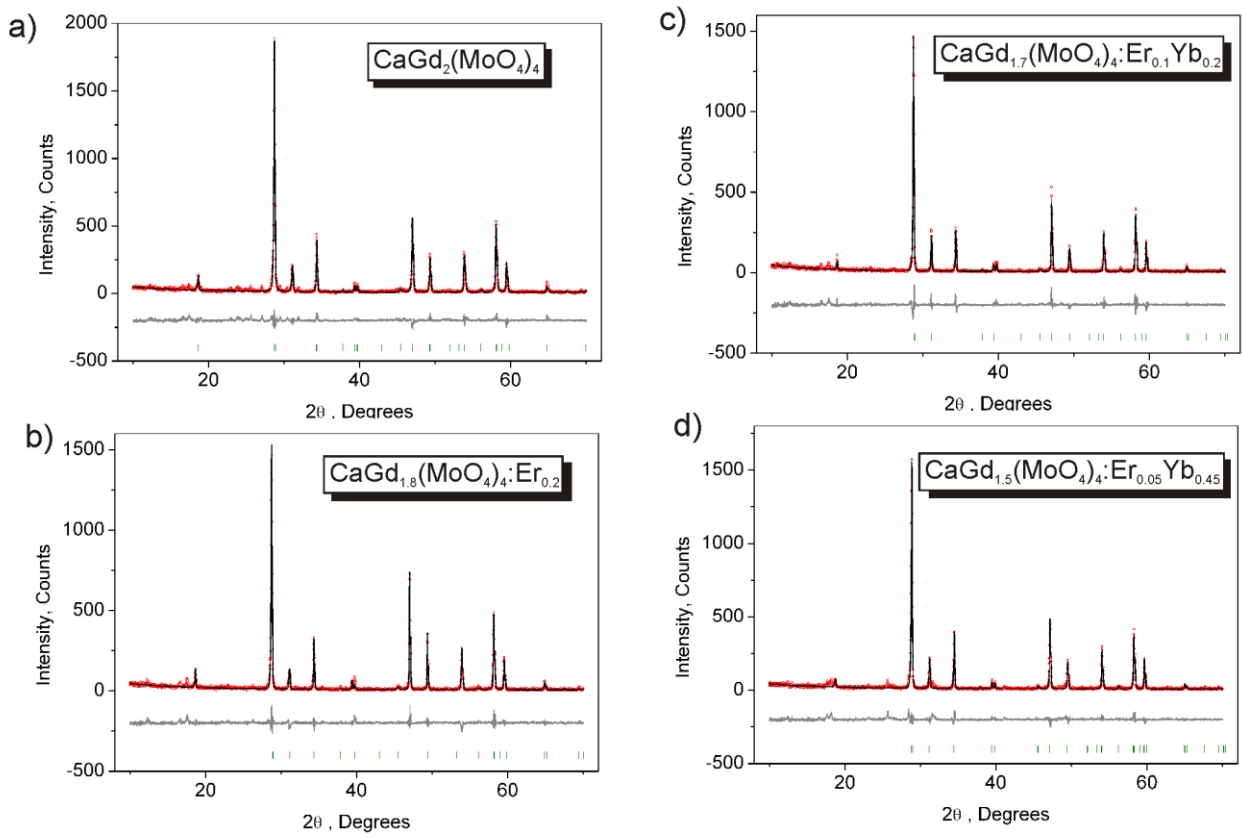


Fig.1.

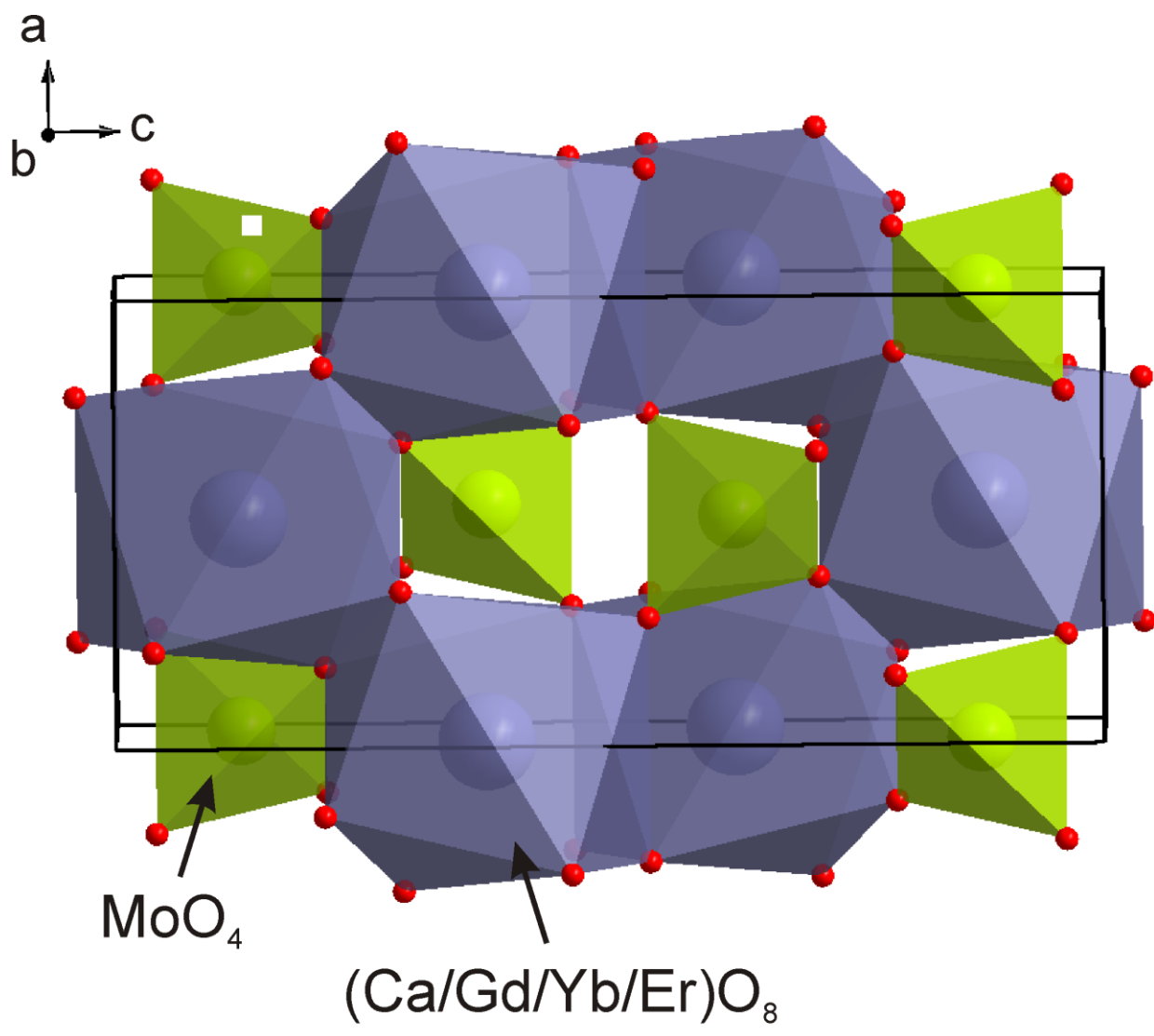


Fig.2.

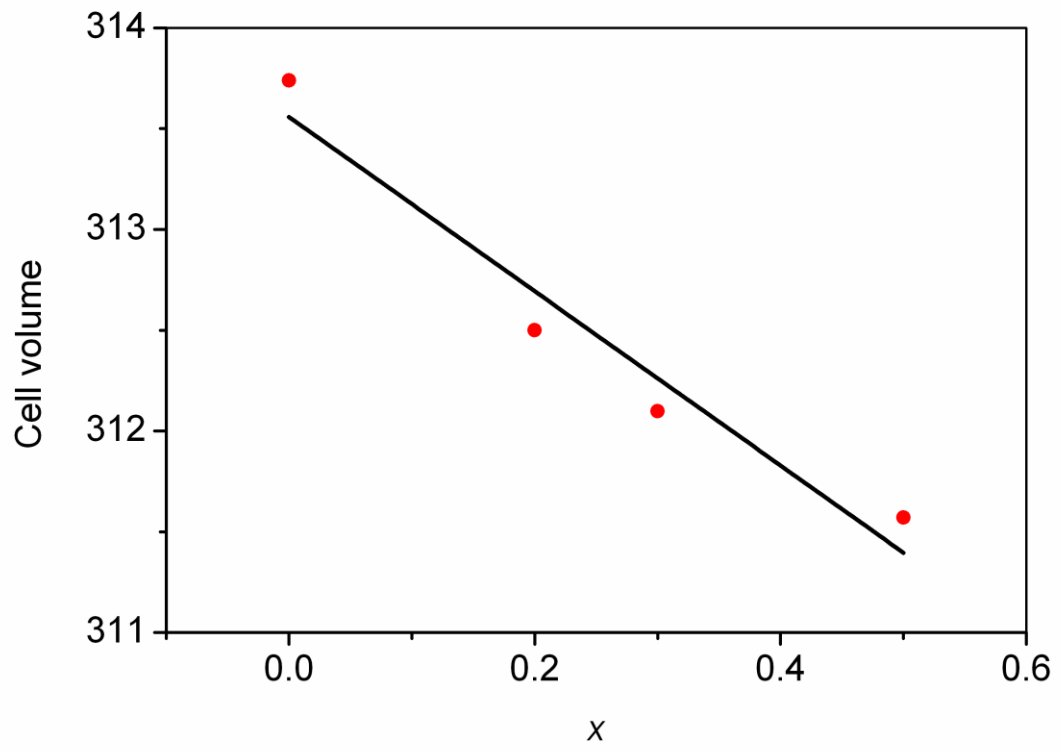


Fig. 3.

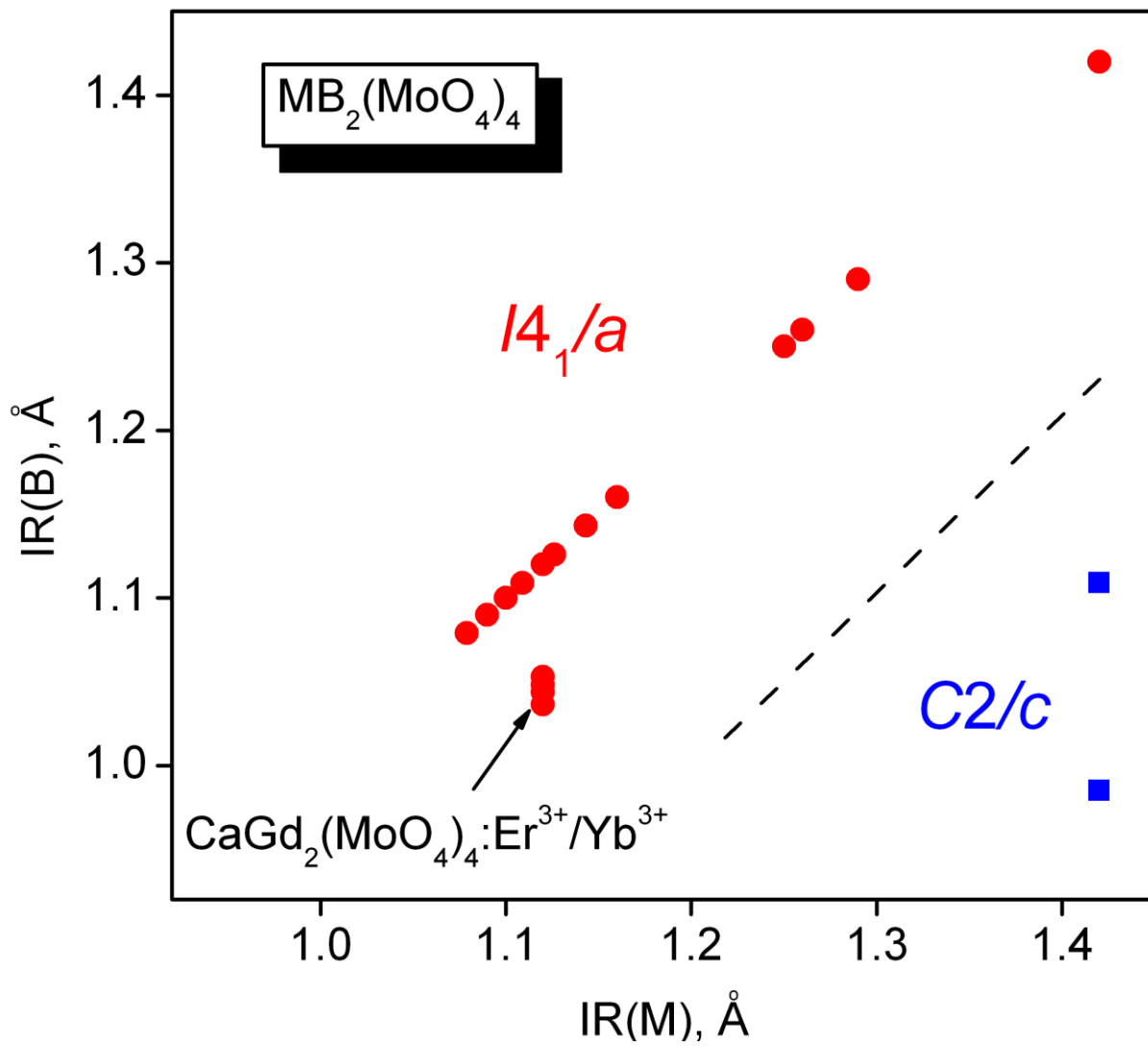


Fig.4.

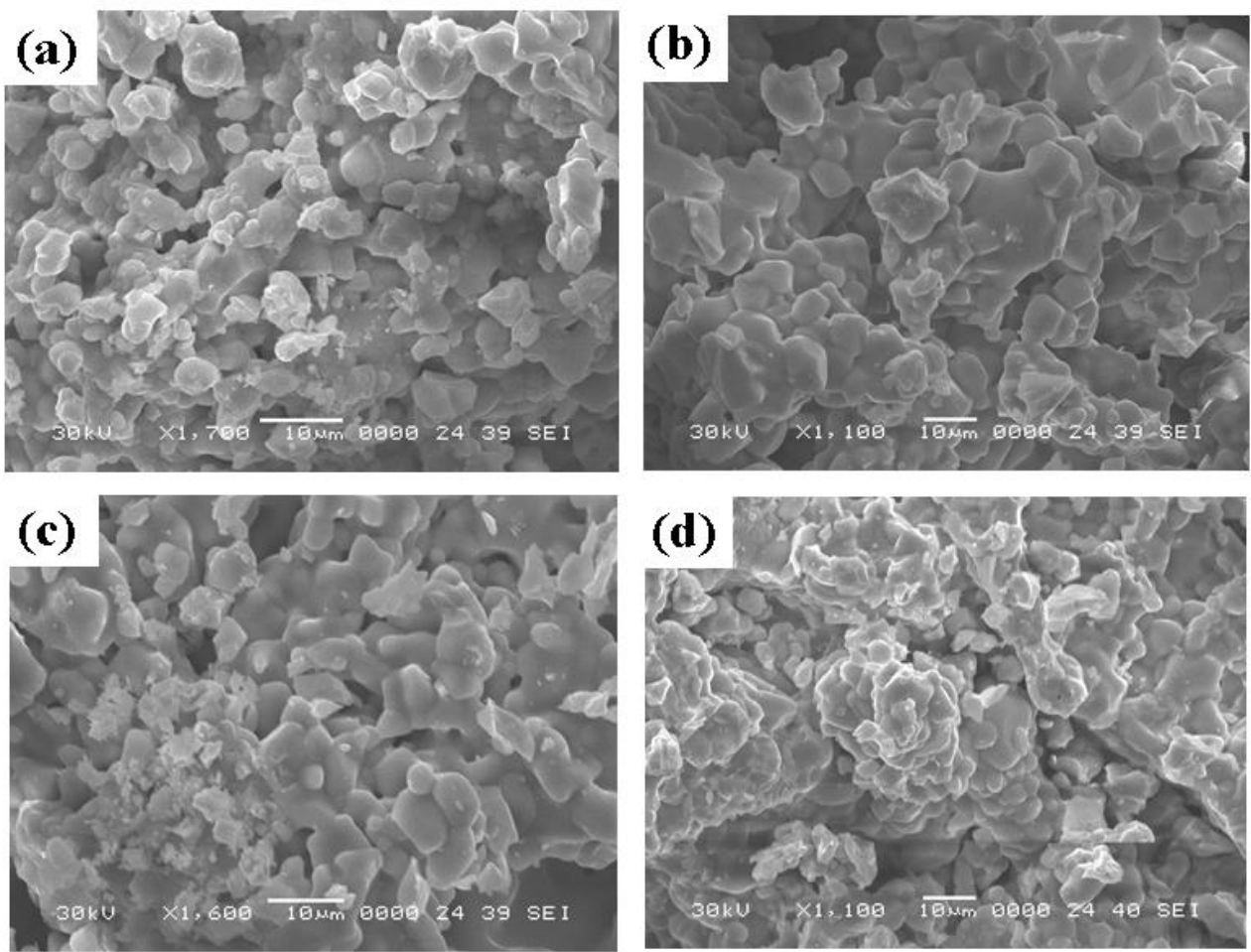


Fig. 5.

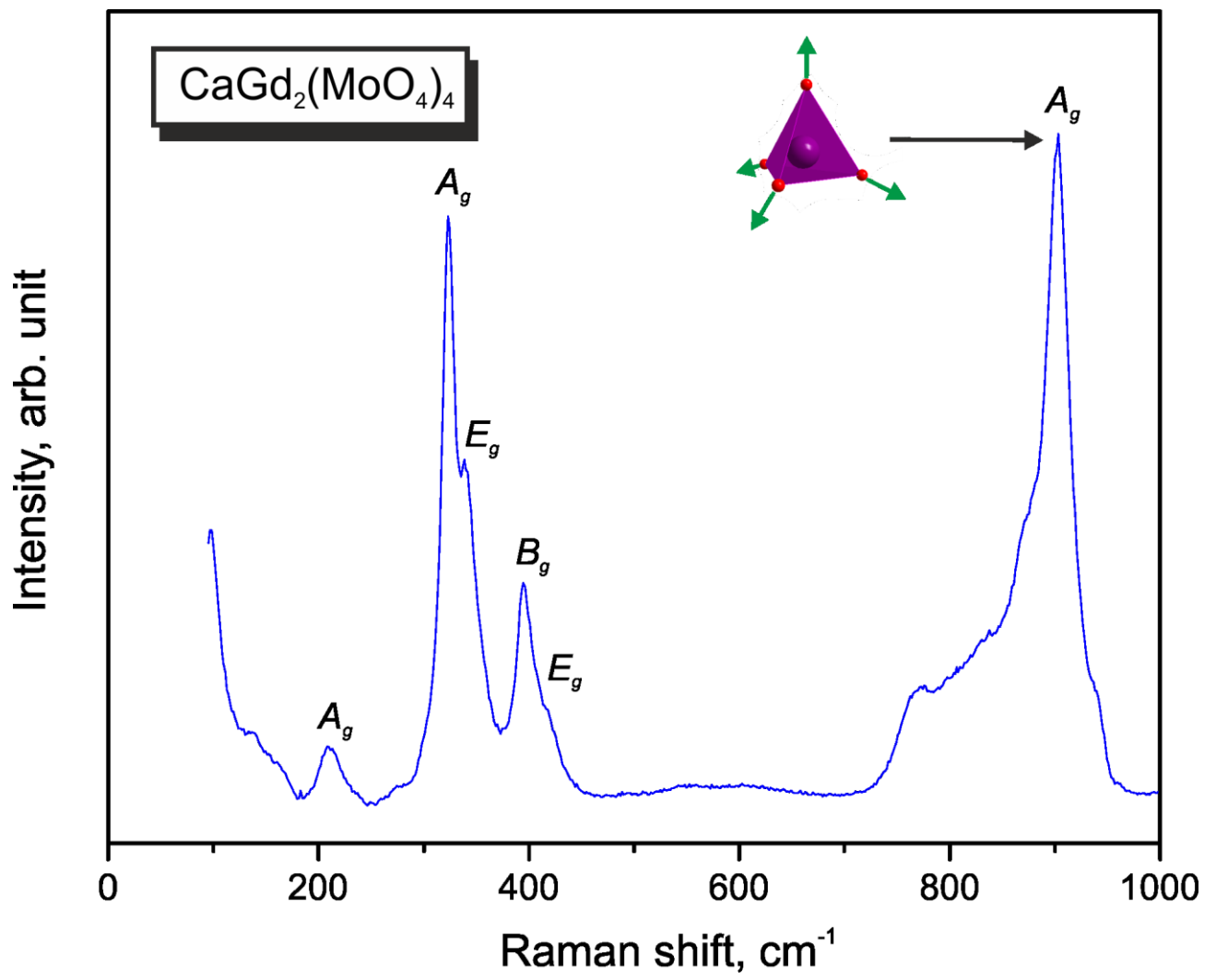


Fig.6.

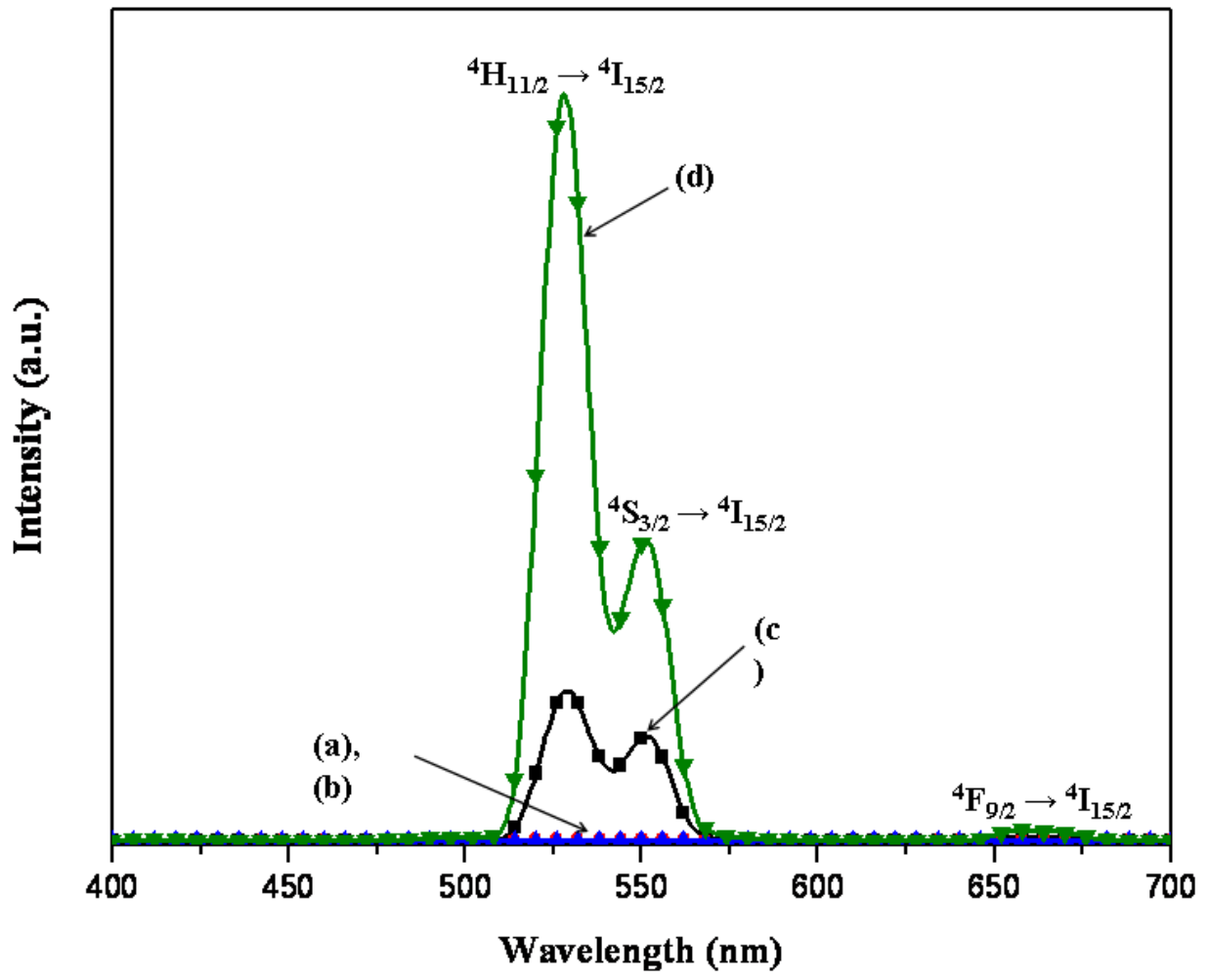


Fig.7.

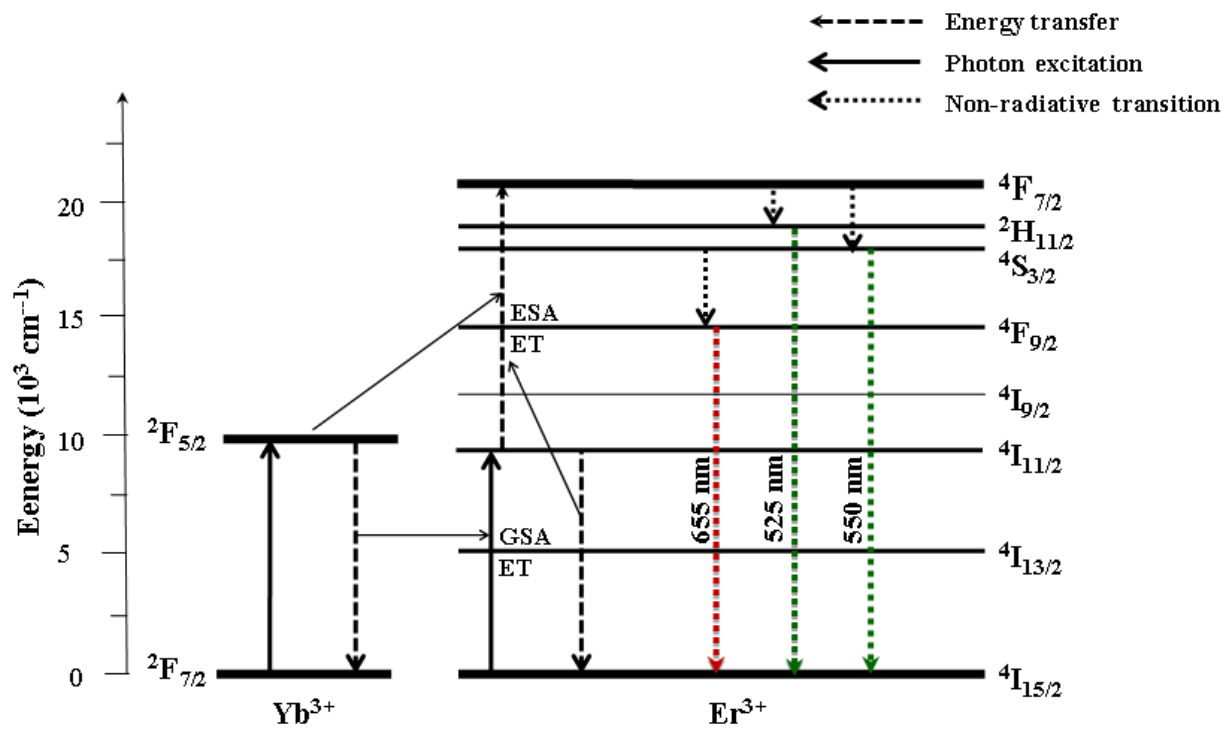


Fig.8.

Supporting Information

Microwave sol-gel synthesis of microcrystalline $\text{CaGd}_2(\text{MoO}_4)_4:\text{Er}^{3+}/\text{Yb}^{3+}$ phosphors and their upconversion photoluminescence properties

Chang Sung Lim¹, Victor Atuchin^{2,3,4,*}, Aleksandr Aleksandrovsky^{5,6}, Maxim Molokeev^{7,8},
Aleksandr Oreshonkov^{6,9}

¹Department of Advanced Materials Science & Engineering, Hanseo University, Seosan 356-706, Republic of Korea

²Laboratory of Optical Materials and Structures, Institute of Semiconductor Physics, SB RAS, Novosibirsk 630090, Russia

³Functional Electronics Laboratory, Tomsk State University, Tomsk 634050, Russia

⁴Laboratory of Semiconductor and Dielectric Materials, Novosibirsk State University, Novosibirsk 630090, Russia

⁵Laboratory of Coherent Optics, Kirensky Institute of Physics, SB RAS, Krasnoyarsk 660036, Russia

⁶Department of Photonics and Laser Technologies, Siberian Federal University, Krasnoyarsk 660079, Russia

⁷Laboratory of Crystal Physics, Kirensky Institute of Physics, SB RAS, Krasnoyarsk 660036, Russia

⁸Department of Physics, Far Eastern State Transport University, Khabarovsk 680021, Russia

⁹Laboratory of Molecular Spectroscopy, Kirensky Institute of Physics, SB RAS, Krasnoyarsk 660036, Russia

Structural information in four cif files.

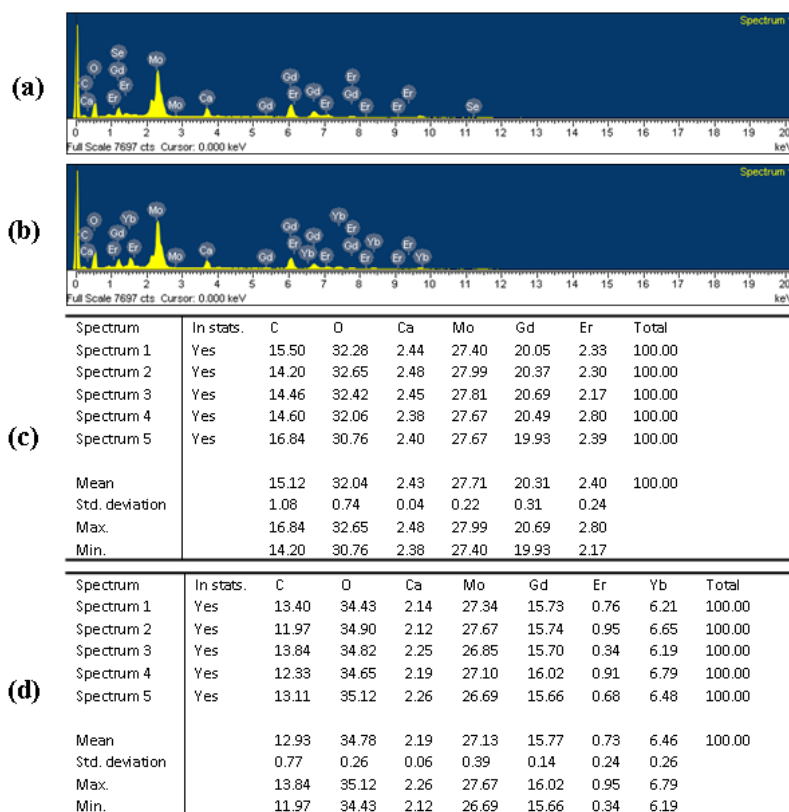


Fig. 1S: Energy-dispersive X-ray spectroscopy patterns of the synthesized (a) $\text{CaGd}_{1.8}(\text{MoO}_4)_4:\text{Er}_{0.2}$ and (b) $\text{CaGd}_{1.5}(\text{MoO}_4)_4:\text{Er}_{0.05}\text{Yb}_{0.45}$ particles, and quantitative compositions of (c) $\text{CaGd}_{1.8}(\text{MoO}_4)_4:\text{Er}_{0.2}$ and (d) $\text{CaGd}_{1.5}(\text{MoO}_4)_4:\text{Er}_{0.05}\text{Yb}_{0.45}$ particles.

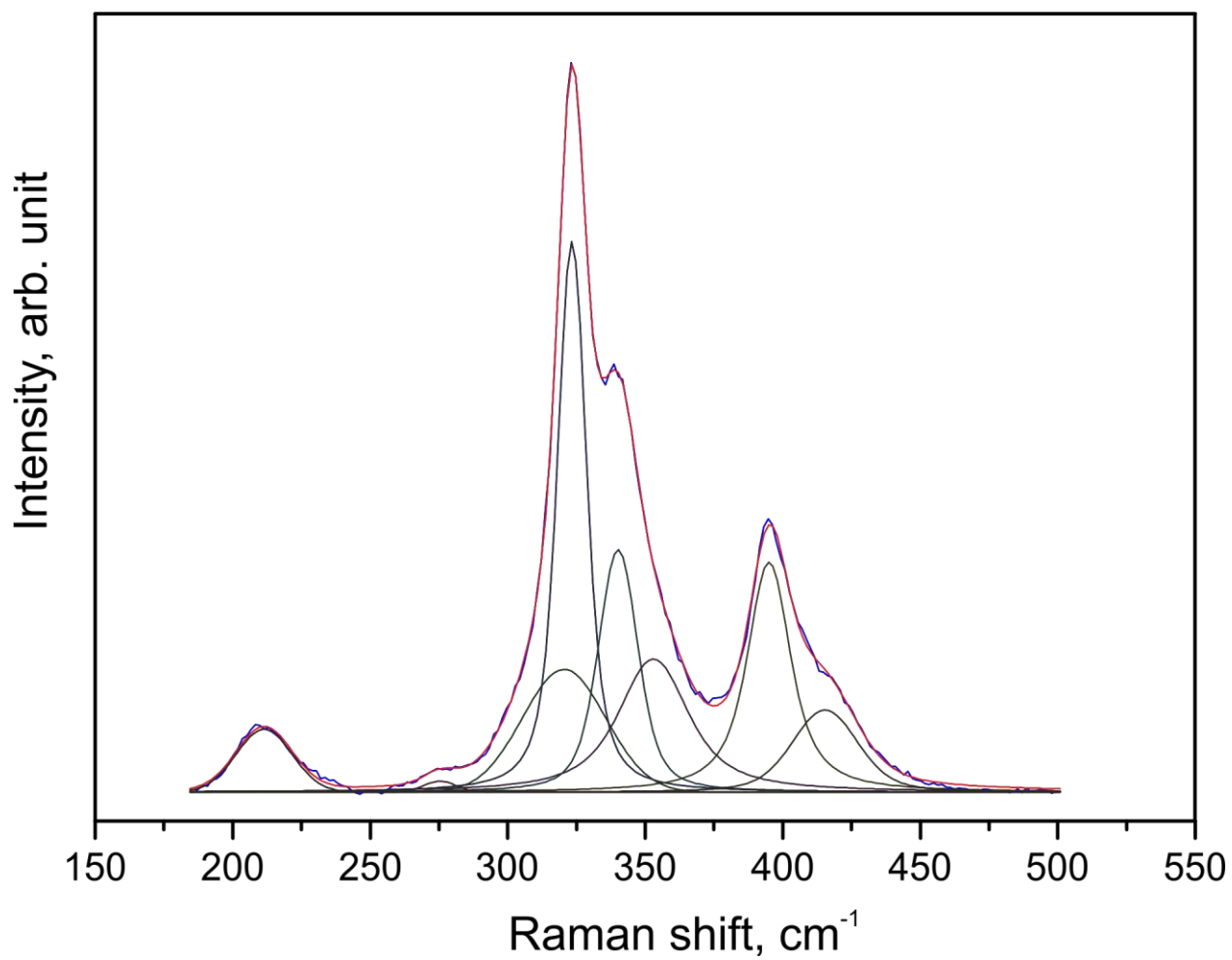


Fig. 2S: Raman spectrum of $\text{CaGd}_2(\text{MoO}_4)_4$ over low wavenumber range.

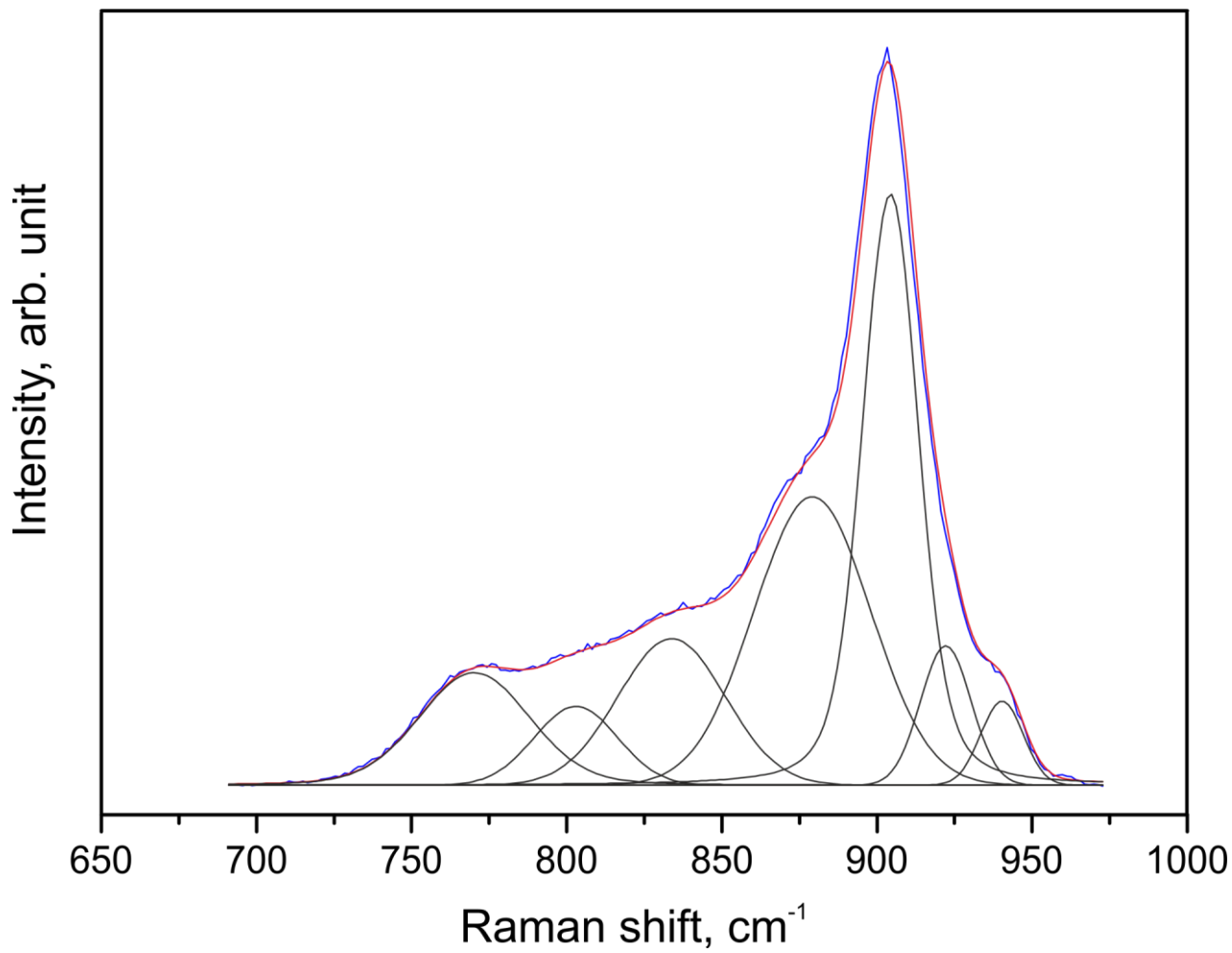


Fig. 3S: Raman spectra of $\text{CaGd}_2(\text{MoO}_4)_4$ over high wavenumber range.

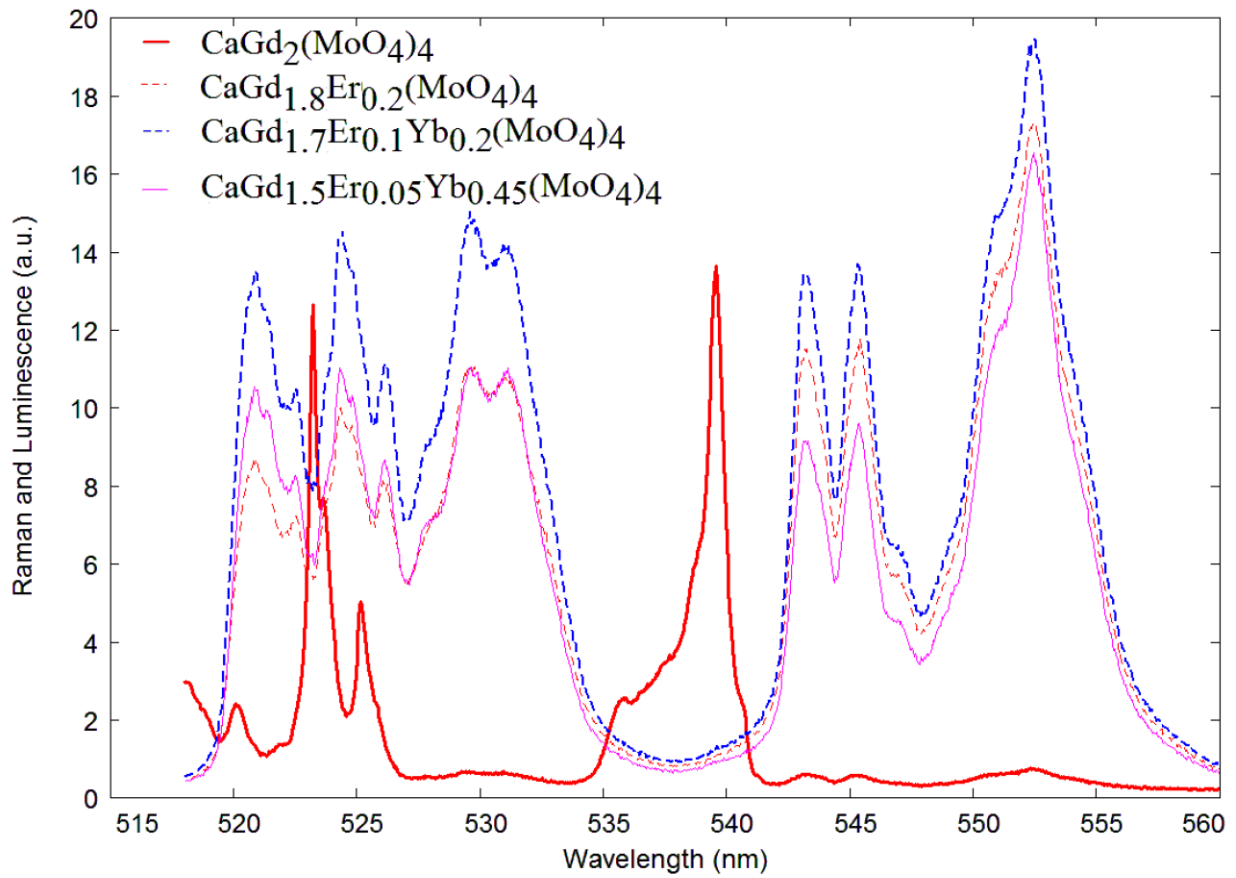


Fig. 4S. Emission spectra of undoped (red) and erbium and ytterbium doped samples under 514.5 nm excitation. Spectrum of undoped sample contains only Raman contribution. Luminescence of erbium ions at ${}^2\text{H}_{11/2} \rightarrow {}^4\text{I}_{15/2}$ and ${}^4\text{S}_{3/2} \rightarrow {}^4\text{I}_{15/2}$ transitions completely dominate in the spectra of doped samples.